HHS Public Access

Author manuscript

Cell Rep. Author manuscript; available in PMC 2023 December 25.

Published in final edited form as:

Cell Rep. 2023 November 28; 42(11): 113338. doi:10.1016/j.celrep.2023.113338.

Anti-inflammatory effects of hunger are transmitted to the periphery via projection-specific AgRP circuits

Michelle L. Klima[1,2,5], **Kayla A. Kruger**[1,5], **Nitsan Goldstein**[1,2], **Santiago Pulido**[1], **Aloysius Y.T. Low**[1], **Charles-Antoine Assenmacher**[3], **Amber L. Alhadeff**[2,4,*], **J. Nicholas Betley**[1,2,6,*]

[1]Department of Biology, University of Pennsylvania, Philadelphia, PA 19104, USA

[2]Department of Neuroscience, University of Pennsylvania, Philadelphia, PA 19104, USA

[3]Comparative Pathology Core, Department of Pathobiology, University of Pennsylvania School of Veterinary Medicine, Philadelphia, PA 19104, USA

[4]Monell Chemical Senses Center, Philadelphia, PA 19104, USA

[5]These authors contributed equally

[6]Lead contact

SUMMARY

Caloric restriction has anti-inflammatory effects. However, the coordinated physiological actions that lead to reduced inflammation in a state of caloric deficit (hunger) are largely unknown. Using a mouse model of injury-induced peripheral inflammation, we find that food deprivation reduces edema, temperature, and cytokine responses that occur after injury. The magnitude of the anti-inflammatory effect that occurs during hunger is more robust than that of non-steroidal anti-inflammatory drugs. The effects of hunger are recapitulated centrally by activity in nutrient-sensing hypothalamic agouti-related protein (AgRP)-expressing neurons. We find that AgRP neurons projecting to the paraventricular nucleus of the hypothalamus rapidly and robustly reduce inflammation and mediate the majority of hunger's anti-inflammatory effects. Intact vagal efferent signaling is required for the anti-inflammatory action of hunger, revealing a brain-to-periphery pathway for this reduction in inflammation. Taken together, these data begin to unravel a potent anti-inflammatory pathway engaged by hypothalamic AgRP neurons to reduce inflammation.

Graphical abstract

*Correspondence: aalhadeff@monell.org (A.L.A.), jnbetley@sas.upenn.edu (J.N.B.).

AUTHOR CONTRIBUTIONS

M.L.K., S.P., A.L.A., and J.N.B. initiated the project. M.L.K., K.A.K., A.L.A., and J.N.B. prepared the manuscript with comments from all authors. M.L.K., K.A.K., C.-A.A., S.P., and A.L.A. performed experiments. M.L.K., K.A.K., A.Y.T.L., and N.G. performed surgical procedures. M.L.K., K.A.K., A.L.A., and J.N.B. designed experiments and analyzed data.

SUPPLEMENTAL INFORMATION

Supplemental information can be found online at https://doi.org/10.1016/j.celrep.2023.113338.

DECLARATION OF INTERESTS

The authors declare no competing interests.

INCLUSION AND DIVERSITY

We support inclusive, diverse, and equitable conduct of research.

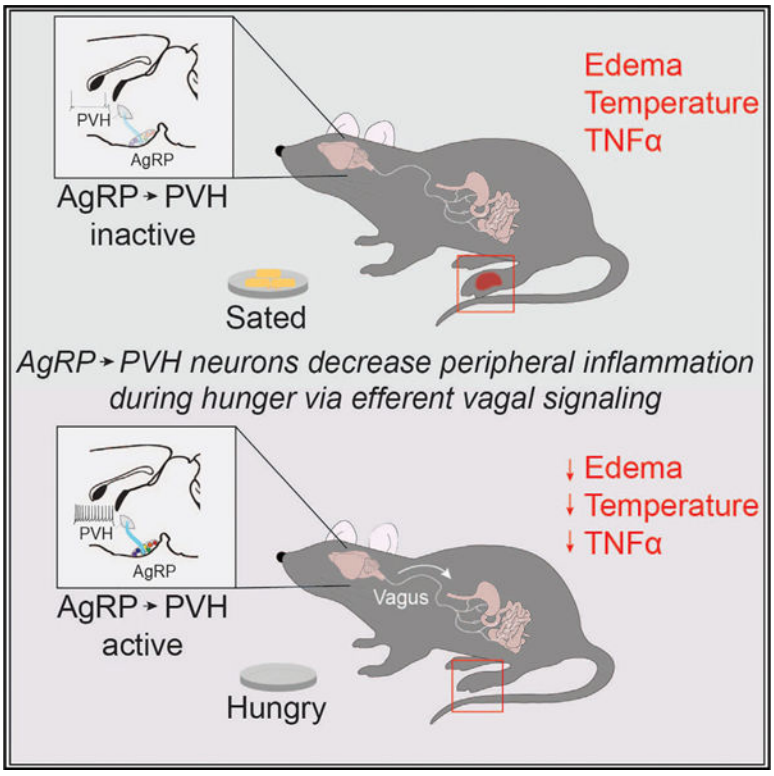

In brief

Klima et al. describe a neural mechanism underlying hunger's potent anti-inflammatory effects. AgRP neurons projecting to the paraventricular hypothalamus inhibit peripheral inflammation through efferent vagal signaling. These findings highlight the central role of hunger circuits in the rapid and robust control of peripheral inflammation.

INTRODUCTION

Calorie restriction leads to a series of complex physiological changes in both the central nervous system (CNS) and the periphery that can be advantageous for inhibiting inflammation and improving related comorbidities.[1,2] However, since there are so many diverse effects of hunger, isolating the mechanisms that inhibit inflammation has been challenging. Therefore, developing an understanding of how calorie restriction influences inflammation should be a goal of research aimed at enhancing health and longevity.

How might caloric restriction influence peripheral inflammation? Fasting inhibits the activation of inflammasomes[3–5] and reduces the production and release of pro-inflammatory cytokines.[6–9] Food deprivation may also influence the immune system through changes in peripheral hormone levels, gene expression, metabolic factors, and/or central hunger circuits.[10–12] Although both peripheral and central pathways influence inflammation, hunger circuits in the CNS likely play an important role, as manipulation of gene expression in hypothalamic agouti-related protein (AgRP)-expressing neurons can influence adaptive

immune responses.[13] Therefore, we sought to identify the central-to-peripheral pathways that mediate the effects of food deprivation.

Here, we found that food deprivation robustly and reliably inhibited inflammation regardless of age, sex, or body weight, an effect that was more potent than standard anti-inflammatory drugs. We also found that these anti-inflammatory effects of food restriction occur through vagal efferent signaling. The effects of calorie deprivation can be rapidly (within 1 h) recapitulated by engaging hypothalamic AgRP neuron activity, and these effects are dominated by AgRP neurons that project to the paraventricular nucleus of the hypothalamus (PVH). These findings highlight a neural circuit that suppresses inflammation, raising the possibility that endogenous neural networks can be leveraged to develop anti-inflammatory therapies.

RESULTS

Hunger reduces inflammation in response to noxious chemical stimuli

Inflammation can be modeled by assessing injury-induced inflammatory responses following injection of an irritant such as formalin or complete Freund's adjuvant (CFA) into a rodent paw. Because hunger has a profound effect on inflammation and inflammatory pain responses,[14] we evaluated the ability of food deprivation to influence these models of injury-induced inflammation (Figures 1A and S1A). We found that food deprivation robustly suppressed paw inflammation. Specifically, food deprivation attenuated injury-induced inflammation resulting from both CFA and formalin paw injections by approximately 50% (Figures 1B–1D, S1B, and S1C). This effect on inflammation was sustained, as chronic food restriction reduced CFA-induced paw inflammation for up to 1 week (168 h; Figure S1D).

We next evaluated whether biological variables such as sex, age, and body weight influence the effect of food deprivation on CFA-induced inflammation. Across experimental cohorts, we consistently found that food deprivation reduced paw volume after an injection of CFA (Figure S1E). Given that there are sex differences in immune signaling,[15–17] we examined how hunger influences inflammation in both male and female mice. As previously reported, we observed that female mice had a larger paw volume after a CFA injection[17,18]; however, food deprivation reduced inflammation to a similar magnitude in both male and female mice (Figure S1F). The immune system can also be influenced by age[19,20] or body weight.[5,21] We therefore quantified paw volume after CFA injection in mice at varying ages and body weights. Although age influences the inflammatory response to CFA, food deprivation reduced CFA-induced inflammation to the same extent across all age and body weight groups (Figures S1G and S1H). Together, these data demonstrate that food deprivation robustly and consistently inhibits peripheral inflammation across multiple biological variables.

Local inflammation is characterized by increases in swelling (edema), redness, temperature, and cytokine/chemokine infiltration.[22,23] We observed that the reduction in CFA-induced paw volume causedby food deprivation was directly related to the levels of edema (Figure 1E) and not by histopathological changes at the injury site,[24] as measured by qualitative suppurative inflammation scores and $CD45^+$ cell staining in the paw (Figures 1F and 1G).

We observed a robust reduction in levels of the inflammatory cytokine tumor necrosis factor α (TNF-α) at the site of the injury (Figure 1H), suggesting that hunger reduces the expression of inflammatory cytokines. Additionally, food deprivation dramatically reduced paw temperature following CFA injection (Figures 1I, 1J, and S1I).

Because of our observations that food deprivation is a highly reliable, reproducible, and potent mechanism to attenuate injury-induced inflammation, we next wanted to determine how it compares to standard treatments for inflammation. We found that food deprivation has a larger anti-inflammatory effect than typical doses of non-steroidal anti-inflammatory drugs (NSAIDs). Indeed, food deprivation reduced CFA-induced paw volume 20% more than administration of ketoprofen or ketorolac (Figures 1K and S2A–S2C). Taken together, our observations suggest that the endogenous mechanisms activated by hunger include a powerful anti-inflammatory signal that can be readily observed and investigated in our paw injury model.

Descending vagal signaling mediates the anti-inflammatory effects of hunger

Do the anti-inflammatory effects of hunger require signaling between the brain and the periphery? Vagal immune-brain signaling plays an important role in inflammatory responses[25–27] by providing bidirectional communication between the periphery and the CNS. The afferent neurons carry interoceptive sensory signals to the brain, while the efferent neurons send the appropriate motor or physiological response to the periphery (Figure 2A).[25,28] We therefore asked if vagal signaling is required for the suppression of inflammation by food deprivation. We first lesioned both afferent and efferent vagal pathways by performing a complete subdiaphragmatic vagotomy (VGX) (Figure 2B). VGX attenuated the ability of food deprivation to suppress inflammation (Figure 2C). This effect is recapitulated by intraperitoneal (i.p.) injection of a cocktail of antagonists for corticotropin-releasing factor (CRF), adrenergic, and cholinergic receptors that block vagal efferent output (Figure 2D).[29] We next performed a selective lesion of afferent vagal fibers by treatment with capsaicin, which causes cytotoxicity of TRPV1-expressing neurons.[30,31] Ablation of afferent fibers did not change the ability of hunger to suppress inflammation (Figure 2E), although it was effective at influencing hunger and nociceptive responses (Figures 2F–2H). Taken together, these findings suggest that vagal efferent signaling is necessary for hunger to suppress inflammation.

AgRP neuron activity recapitulates the effect of hunger on inflammation

Because the cell bodies of vagal efferent neurons reside in the brain, our findings suggest that central circuits mediate the suppression of inflammation during hunger. We next explored the possibility that neural circuits activated by food deprivation attenuate inflammation. AgRP neurons are activated by food deprivation,[32–35] and activity in these neurons inhibits formalin- and CFA-induced inflammatory pain.[14] We therefore investigated if activation of AgRP neurons influences CFA-induced inflammation. We chemogenetically or optogenetically activated AgRP neurons and measured all aspects of inflammation. As previously shown,[36] chemogenetic activation by designer receptors exclusively activated by designer drugs (DREADDs; hM3Dq) led to robust food intake (Figures 3A and 3B). Chemogenetic AgRP neuron activation also attenuated CFA-induced paw volume (Figure

3C), an effect that was not observed in control (mCherry-expressing) mice (Figure 3D). Similarly, optogenetic activation of AgRP neurons (Figure 3E), which also drives food intake (Figure 3F), attenuated inflammation following CFA paw injection (Figures 3G and 3H). Activating AgRP neurons also reduced the CFA-induced increase in paw temperature and circulating levels of TNF-α (Figures 3I–3L). Importantly, we find that chemogenetic inhibition of AgRP neurons with the DREADD hM4Di (Figure 3M) during food deprivation diminishes the reduction in paw volume and paw temperature normally observed in hunger (Figures 3N–3P), demonstrating that activity in AgRP neurons is essential for the anti-inflammatory effects of hunger. Together, these observations reveal that activity in AgRP neurons initiates a rapid (<1 h) reduction in multiple measures of inflammation.

AgRP→PVH and AgRP→PBN subpopulations reduce CFA-induced paw volume

AgRP neurons project to multiple targets throughout the brain.[37,38] Because AgRP neurons form anatomical subpopulations with minimal collateralization,[37] we were able to individually stimulate each axon projection to explore where hunger information is transmitted to suppress inflammation. We performed a systematic analysis of the major AgRP neuron projection subpopulations by activating individual axon projections in *ad libitum*-fed mice and measuring CFA-induced changes in paw volume (Figure 4A). We found that activation of AgRP neurons that project to either the paraventricular hypothalamic nucleus (PVH) or the parabrachial nucleus (PBN) were capable of reducing paw volume after CFA treatment (Figures 4B, 4C, and S3). The projection to the PVH had a larger magnitude effect that more closely resembled the effects observed in food deprivation (Figure 4B). Activation of AgRP projections to the PVH also suppressed the increase in temperature normally associated with injury (Figures 4D and 4E), unlike the neurons that project to the PBN (Figures 4F and 4G). Taken together, these results suggest that the inflammatory action of AgRP neurons is distributed over two nodes in the brain to which AgRP neurons project and that the AgRP projection to the PVH mediates the bulk of the anti-inflammatory effect of AgRP neurons.

DISCUSSION

Here, we uncover the ability of a central circuit activated by food deprivation to reduce inflammation. We demonstrate that hunger reduces injury-induced peripheral paw inflammation in a vagal-dependent manner. The effect of hunger is mediated by activity in AgRP neurons, which leads to reduced edema, temperature, and cytokine levels. These effects are observed rapidly (within 1 h of AgRP neuron activity starting) and are largely mediated by the activity of AgRP neurons that project to the PVH. Taken together, these findings reveal a central neural circuit that can inhibit peripheral inflammation, providing new insight into how food deprivation reduces inflammation.

Why does food deprivation influence pain, itch, and peripheral inflammation?[14,39] While inflammation is an adaptive response to injury, long-term inflammation and associated behavioral responses can become maladaptive and prevent basic actions necessary for survival. When faced with a homeostatic challenge such as food deprivation, neural circuits prioritize the most salient need. For example, our previous findings show that hunger,

through AgRP→PBN neuron signaling, inhibits long-term inflammatory pain.[14] In fact, AgRP neurons have been broadly implicated in a hierarchical prioritization of behavior, as their activity not only promotes food intake[40,41] but also influences other survival needs such as sleep, fear/anxiety, and aggression.[42–47] Thus, an emerging concept in the neurobiology of homeostasis suggests that need-sensing neurons, such as AgRP neurons, use multiple mechanisms to inhibit competing behavioral drives.

While AgRP neuron stimulation is well known to influence behavior, the current work describes physiological changes that are driven by activity in AgRP neurons. Specifically, we show that AgRP neuron stimulation attenuates multiple measures of inflammation following paw injections of noxious stimuli. Previous studies have shown that AgRP neuron activity can also influence physiological measures such as metabolism,[36] glucose homeostasis,[48,49] adaptive immunity,[13] activation of the HPA axis,[50,51] and autonomic nerve activity.[52] These widespread effects that result from AgRP neuron activity highlight the pivotal role of these neurons in influencing both physiology and behavior.

How do so few neurons influence so much biology? The anatomical configuration of AgRP circuits lends a logic that can promote both parallel and redundant as well as segregated and distinct functional consequences. For example, AgRP neuron projections to the bed nuclei of the stria terminalis (BNST), the paraventricular thalamic nucleus (PVT), the PVH, and the lateral hypothalamus (LH) drive food intake,[37] and similar projections (to the anterior BNST and LH) mediate effects on glucose homeostasis.[49] In contrast, AgRP projections that do not drive food intake filter noxious environmental and physiological stimuli to enable feeding behaviors.[14,46,53,54] Building on our previous work demonstrating a role for AgRP neuron signaling in behavioral responses to pain and itch,[14] the current study identifies a distinct neural circuit architecture that attenuates peripheral inflammation.

How does food deprivation, and AgRP→PVH signaling, ultimately result in reduced inflammation? The effect of central signaling on peripheral injury-induced inflammation necessitates a mechanism (or multiple mechanisms) of hormonal or neural signaling from the brain to the periphery. Systemic control of inflammation can be influenced by the hypothalamic-pituitary-adrenal (HPA) axis.[55] This system originates in the PVH and results in secretion of peripheral anti-inflammatory glucocorticoids. Interestingly, recent work demonstrated that AgRP neurons activate the HPA axis via disinhibition of PVH corticotrophin-releasing hormone-expressing neurons.[50,51] Although we demonstrate that AgRP→PVH neuron activity reduces inflammation, neither corticosterone administration in fed mice nor blocking glucocorticoid signaling in hungry mice influenced inflammation (data not shown). Further, stimulation in AgRP→BNST and AgRP→LH terminal regions also activates the HPA axis to increase plasma corticosterone,[50] yet stimulation of these regions did not reduce peripheral inflammation (Figure 4B). These findings are therefore inconsistent with HPA axis mediation of the anti-inflammatory effects of AgRP neurons. Rather, our data suggest thatvagal efferent signaling mediates the effects of hunger on inflammation,[25–27] adding to the body of literature featuring the contribution of vagal signaling to inflammatory responses.[25–27] It will be imperative for future work to determine how AgRP→PVH neurons communicate with vagal efferent neurons in the hindbrain and

the cellular and molecular mechanisms through which vagal neurotransmission rapidly relays this central signal to inhibit inflammation.

Overall, our findings identify a central circuit for the inhibition of injury-induced inflammation. While it is known that the CNS has bidirectional communication with the immune system, these findings provide new neuron populations, AgRP→PVH and AgRP→PBN, that are capable of reducing localized injury-induced inflammation. By developing an understanding of how central and peripheral signals interact to inhibit inflammation, these experiments provide novel targets for the development of analgesic and anti-inflammatory therapies.

Limitations of the study

Our experiments nucleate a circuit-based understanding of the anti-inflammatory effects of hunger; however, a limitation of these studies is that we have not uncovered the complete circuit and molecular mechanisms of this effect. While our current work indicates that AgRP neurons that project to the PVH are important for reducing peripheral inflammation, many questions remain. What transmitters and receptors are important for the anti-inflammatory effects of hunger? What cells in the PVH mediate this effect? And through which circuits or networks is this effect signaled to vagal efferents and, ultimately, the periphery? Addressing these next-step questions will be important to better understand the anti-inflammatory effects of hunger. Furthermore, given that inflammation poses a large human health burden, it will be important to determine if the same AgRP→PVH pathway is broadly important for the inhibition of systemic inflammation, neuroinflammation, and/or inflammation associated with disease.

STAR★METHODS

RESOURCE AVAILABILITY

Lead contact—Further information and requests for resources and reagents should be directed to and will be fulfilled by the lead contact, J. Nicholas Betley (jnbetley@sas.upenn.edu).

Materials availability—This study did not generate any new reagents.

Data and code availability

- The data reported in this paper will be shared by the lead contact upon request.
- This paper does not report original code.
- Any additional information required to reanalyze the data reported in this work paper is available from the lead contact upon request.

EXPERIMENTAL MODEL AND SUBJECT DETAILS

Mice were group housed on a 12 h light/12 h dark cycle with *ad libitum* access to food (Purina Rodent Chow, 5001) and water unless otherwise noted. Vivarium rooms are controlled between 21.5° and 22.3°C with maintained negative pressure between −191.6

and 109.5 Pascal. Group housed adult male and female mice (at least 8 weeks old) were used for experimentation. *Agrp*-IRES-Cre (Jackson Labs 012899, *Agrp*$^{tm1(cre)Lowl}$/J),[56] Ai32 (Jackson Labs 012569, B6; 129S-Gt(ROSA)26Sor$^{tm32(CAG–COP4*H134R/EYFP)Hze}$/J),[57] Ai9 (Jackson Labs 007909, B6.Cg-GT(ROSA)26Sortm9(CAG-tdTomato)Hze/J),[57] CD1 (Charles River 022), *R26-LSL-Gi-DREADD* (Jackson Labs 026219, B6N.129-Gt(ROSA)26Sor$^{tm1(CAG–CHRM4*,–mCitrine)/Ute}$/J),[58] and C57BL6 (Jackson Labs 000664) mice were used for experimentation. All mice were habituated to handling and experimental conditions prior to experiments. We performed experiments in both male and female mice and did not observe any trends or significant sex differences. Thus, to ensure our studies were appropriately powered and to minimize the number of subjects who had to undergo painful procedures, we combined males and females for analyses in all experiments. All procedures were approved by the University of Pennsylvania Institutional Animal Care and Use Committee.

METHOD DETAILS

Recombinant Adeno-Associated Virus (rAAV) Constructs and Production: The following Cre-dependent rAAV vectors were used: AAV5.Ef1a.doublefloxed-hChR2(H134R)-WfP-wPRE-HGHpA (titer: 1×10^{13} vg/mL, Addgene 20298), AAV5.hSyn.DIO.hM3D(Gq).mcherry (titer: 7×10^{12} vg/mL, Addgene 44361), AAV8.hSyn.DIO.mcherry (titer: 1×10^{13} vg/mL, Addgene 50459). These viruses were purchased from Addgene. WPRE, woodchuck hepatitis virus response element. ChR2, channelrhodopsin-2. hSyn, human Synapsin 1 promoter. DIO, double-floxed inverse orientation. hM3, human M3 muscarinic receptor.

Viral injections and fiber optic placement—Mice were anesthetized with isoflurane (1.5%–3%, Clipper, 0010250) and placed into a stereotaxic apparatus (Stoelting, 51725D). Viral injections were performed as previously described.[14] For somatic stimulation of AgRP neurons, *Agrp*-IRES-Cre mice were crossed with Ai32 mice to express ChR2 in AgRP neurons. A unilateral optical fiber (200-μm core, NA 0.37, ThorLabs, FT200UMT) in a fiber ferrule (Kientech, FZI-LC-230) was placed over the arcuate hypothalamic nucleus (ARC) at bregma −1.35 mm, midline ±0.25 mm, skull surface −5.8 mm. For axonal stimulation of AgRP neurons, a rAAV encoding Cre-dependent ChR2 was bilaterally injected into the ARC of *AgRP-IRES-Cre* mice using the aforementioned ARC injection coordinates (150 nL per site, bilaterally). Optical fibers were implanted unilaterally according to the following coordinates: BNST: bregma +0.85 mm, midline ±0.82 mm, skull surface −3.8 mm; PVH: bregma −0.5 mm, midline ±0.2 mm, skull surface −5.4 mm; PVT: bregma −1.0 mm, midline ±0.0 mm, skull surface −2.7 mm; LH: bregma −1.0 mm, midline ±0.9 mm, skull surface −5.4 mm; CeA: bregma −1.15 mm, midline ±2.4 mm, skull surface −4.25 mm; ARC: bregma −1.35 mm, midline ±0.25 mm, skull surface −5.8 mm; PAG: bregma −4.4 mm, midline ±0.6 mm, skull surface −2.8 mm; lateral PBN: bregma −5.8 mm, midline ±1.2 mm, skull surface −3.7 mm. Fibers were secured to the skull with bone screws and dental cement. Mice were given at least 3 weeks for recovery and transgene expression. For chemogenetic activation of AgRP neurons, Agrp-IRES-Cre mice were bilaterally injected with a virus designed to express the excitatory designer receptor exclusively activated by designer drug

(DREADD), hM3Dq. Post hoc histology was used to confirm virus expression and proper placement of fibers.

Complete subdiaphragmatic vagotomy—Mice were maintained on a liquid diet (Ensure Plus Vanilla, Abbott, 53642) for at least 3 days prior to surgery to promote survival and recovery.[59] Mice were anesthetized with isoflurane (1.5%–3%) and treated with subcutaneous meloxicam (5 mg/kg), bupivacaine (2 mg/kg) and buprenorphine SR (1 mg/kg) analgesia. An abdominal midline incision was made through skin and muscle. The stomach was laporotomized to expose the esophagus, and the dorsal and ventral vagal trunks were then exposed by gently teasing them apart from the esophagus. The vagal trunks were resected and cauterized followed by a pyloroplasty. Control mice received a sham surgery that consisted of all surgical procedures except for the resection and cauterization of the vagus nerve. Functional verification of vagotomy was confirmed by examining CCK-induced anorexia (see below). Histological verification of vagotomy was confirmed using an i.p. injection of 0.1% Fluoro-Gold and examining Fluoro-Gold presence in the dorsal motor nucleus of the vagus (DMX) 5 days post-injection.

Capsaicin-induced afferent vagotomy—4-week-old mice were treated with 3 increasing doses of capsaicin for 2 days to ablate the afferent vagal pathway. Mice were pretreated with an i.p. injection of 0.3 mg/kg atropine 30 min before each capsaicin dose. Mice were maintained at 1.5–3% isoflurane 10 min prior to capsaicin treatment and for 30 min post injection. On day 1, mice received 8 mg/kg capsaicin in the morning and 15 mg/kg in the evening. On day 2, mice received an additional dose of 15 mg/kg capsaicin. Mice were given 4 weeks to recover from the procedure prior to experimentation. Vagal afferent ablation was verified by examining CCK-induced anorexia and acute (hot plate paw withdrawal) and inflammatory (formalin-induced paw licking) pain behavior.

General experimental design—For each experiment described below, our subject numbers were determined by our pilot studies, laboratory publications, and power analyses [power = 0.8, significance level = 0.05, effect sizes = 10–30%]. For within-subject behavioral analyses, all mice received all experimental conditions. For between-subject analyses, mice were randomly assigned to experimental condition. For all behavioral experiments, virus expression, fiber placements, and/or cannula placements were verified postmortem, and any mice with viral expression or implants outside of the area of interest were excluded from all analyses.

Induction of peripheral inflammation by noxious chemical stimuli—To induce inflammation, mice were injected subcutaneously in the dorsal hindpaw with 20 μL of 2% formalin or saline (control). For an additional model of inflammation, mice were injected subcutaneously in the plantar hindpaw with 30 μL of 1:1 ratio of Complete Freund's Adjuvant (CFA) or saline. Doses and volumes of chemicals were based on previous work from our lab and others.[14,60–63]

***In Vivo* photostimulation—**Photostimulation of AgRP neurons was performed as previously described, with 10 ms pulses at 20 Hz for 1 s, repeated every 4 s[40]. The output beam from a diode laser (450 nm, Opto Engine) was controlled by a microcontroller

(Arduino Uno) running a pulse generation script. The laser was coupled to a multimode optical fiber (200-μm core, NA 0.37, Doric) with a 1.25 mm OD zirconium ferrule (Kientech) and mating sleeve that allowed delivery of light to the brain by coupling to the implanted ferrule-capped optical fiber in the mouse. Power was set to ensure delivery of at least 2 mW/mm^2 to AgRP soma and at least 5 mW/mm^2 to the center of the AgRP neuron projection fields using the following software:

https://web.stanford.edu/group/dlab/cgi-bin/graph/chart.php.

AgRP photostimulation-induced food intake measurements—To functionally verify our AgRP neuron stimulation, we measured 1-h AgRP neuron stimulation-evoked food intake as previously described.[40] At least one week following ARC fiber optic implant and 3 weeks following AgRP axonal subpopulation fiber optic implant, *Agrp*-IRES-Cre x Ai32 mice were allowed to habituate for at least 1 h to a chamber with *ad libitum* access to chow and water. Following the habituation period, food intake was measured for 1 h to establish a pre-stimulation baseline. Photostimulation was performed during the next hour as described above. After each hour, food intake was measured. For somatic AgRP neuron stimulation, only mice that consumed >0.6 g of chow were included in experiments. Food intake evoked by stimulation of each AgRP neuron projection subpopulation was measured and reported in Figure S3A.

AgRP chemogenetic stimulation-induced food intake measurements—To functionally verify our AgRP neuron activation via chemogenetic activation, we measured food intake 1 h after activation of AgRP neurons by clozapine-N-oxide (CNO).[36] At least three weeks following ARC hM3D injections, *Agrp*-IRES-Cre mice received an i.p. injection of CNO (1 mg/kg) or saline and were given 15 min to habituate to a chamber with access to water. Chow was then added to the chamber and food intake was measured after 1 h. Feeding assays were performed in a counterbalanced manner so that each mouse received both a CNO and saline injection on different days. Only mice that consumed >0.6 g of chow during 1 h of AgRP neuron chemogenetic activation were included in experiments.

Food deprivation—For 24-h food deprivation, mice were placed in a new cage with alpha-dri bedding and water, but no food, 24 h prior to experimentation. For chronic food restriction, mice were weighed at the same time each day and given chow once daily (1.5–3.0 g) after experimentation to maintain 85%–90% of their free-feeding body weight.

Functional verification of capsaicin vagotomy: Effect of CCK on food intake: Sham or capsaicin-treated mice were overnight food deprived and given i.p. injections of CCK (10 mg/kg in saline). Food intake was measured after 30 min.

Quantification of inflammation

Paw volume measurements: Mice were anesthetized with 1.5–3% isoflurane for a baseline paw volume measurement as well as for inflammation-induced paw volume measurements. The plethysmometer (Ugo Basile, Italy, 37140) water cell was filled with a saline solution to create a visible meniscus. Before each trial, the plethsymometer was calibrated with a 0.5 mL calibrating weight. The anesthetized mouse was then positioned so that the

paw was submerged in the solution up to the ankle joint and volume displacement was recorded. Both paws were measured and recorded for all animals. Paw measurements were taken by experimenters blinded to the experimental conditions. Mice were kept in their home cages in the intervening time between paw measurements. Mice with a raw CFA-induced paw volume less than 0.25 mL were eliminated from experiments to ensure all mice had sufficient inflammation to make comparisons. To analyze the data, paw volume measurements after the CFA injection were compared to the pre-injection paw volume using the following equation: $\frac{\text{paw measurement} - \text{baseline paw measurement}}{\text{baseline paw measurement}} \times 100$to obtain a percent increase from baseline.

Paw circumference measurements: Mice were anesthetized with 1.5–3% isoflurane for a baseline paw circumference measurement as well as for inflammation-induced paw circumference measurements. A thin string was tied and marked around the middle of the paw, ensuring all digits were included in the measurement. Marked strings were measured by experimenters blinded to experimental condition.

Paw temperature measurements: Mice were lightly anesthetized with 1.5–3% isoflurane and were positioned with their paw flat on a cardboard surface. Using an FLIR T450sc Professional Thermal Camera, paws were imaged with the temperature sensor positioned in the center of the dorsal hindpaw.

Paw TNFα measurements: Mice were heavily sedated using isoflurane prior to sample collection. Hindpaws were cut at the patella, flash frozen on dry ice in 2 mL tubes, and stored at −80°C. Immediately before performing the ELISA, hindpaw samples were crushed and placed in 2mL tubes with 3 mm zirconium beads, 1 mL of lysis buffer (Invitrogen, FNN0071), and PMSF protease inhibitor (0.5 mM). Samples were shaken in a microtube homogenizer 3 times at 400 rpm for 30 s each cycle. 100 μL of the resulting supernatant was collected for the ELISA and not diluted further. TNF-α concentration was measured using a mouse Quantikine ELISA Kit (R&D Systems, Minneapolis, MN). The sensitivity of this assay is 7 pg/mL.

Histopathology analysis—Animals were anesthetized with 3% isoflurane and the legs were removed at the hip joint. Paws were rinsed in cold PBS then post-fixed in 10% formalin for 72 h on a shaker at room temperature. Paws were then stored in 50% EtOH. After fixation, the entire legs were decalcified in 15% formic acid for 12 h. Two sections at the level of the tarsus, going through the footpad, were obtained and processed for paraffin embedding, sectioning and staining with hematoxylin and eosin. The slides were evaluated semi-quantitatively by board certified veterinary pathologists, blinded to the experimental group distribution.

For immunohistochemistry, 5 μm thick paraffin sections were mounted on ProbeOn slides (Thermo Fisher Scientific). The immunostaining procedure was performed using a Leica BOND RXm automated platform combined with the Bond Polymer Refine Detection kit (Leica #DS9800). Briefly, after dewaxing and rehydration, sections were pretreated with the epitope retrieval BOND ER2 high pH buffer (Leica #AR9640) for 20 min at 98°C.

Endogenous peroxidase was inactivated with 3% H_2O_2 for 10 min at room temperature (RT). Nonspecific tissue-antibody interactions were blocked with Leica PowerVision IHC/ISH Super Blocking solution (PV6122) for 30 min at RT. The same blocking solution also served as diluent for the primary antibody. Rat monoclonal primary antibody against CD45-LCA (BD Biosciences; #553076) was used at a concentration of 1:300 and incubated on the sections for 45 min at RT. A biotin-free polymeric IHC detection system consisting of HRP conjugated goat anti-rat IgG (Vector Laboratories MP-7444) was then applied for 25 min at RT. Immunoreactivity was revealed with the diaminobenzidine (DAB) chromogen reaction. Slides were finally counterstained in hematoxylin, dehydrated in an ethanol series, cleared in xylene, and permanently mounted with a resinous mounting medium (Thermo Scientific ClearVueTM coverslipper). Pooled sections of murine lymphoid tissues, including the cervical and mesenteric lymph nodes and the spleen, served as positive controls. Negative controls were obtained either by omission of the CD45-LCA antibody or replacement with an irrelevant isotype-matched rat monoclonal antibody.

The IHC slides were scanned at 20× magnification using a Leica Aperio AT2 slide scanner (Leica Biosystems, Inc., Buffalo Grove, IL) and image acquisition and analysis was performed with ImageScope (Leica Biosystems, Inc., Buffalo Grove, IL). A single positive pixel count algorithm was generated to quantify the area of CD45-LCA positivity, while the total area of tissue on the slide was measured using a Genie algorithm.

Effect of food deprivation on formalin-induced peripheral inflammation: Food was removed 24 h prior to formalin injection. *Ad libitum* fed mice served as controls. Paw volume and paw circumference were measured prior to injection and 60 min post-injection.

Effect of food deprivation on CFA-Induced peripheral inflammation: Food was removed after mice were injected with CFA. *Ad libitum* fed mice served as controls. Paw volume, circumference, edema score, temperature, and TNFα levels were measured 24 h post-CFA injection.

Effect of refeeding on CFA-Induced peripheral inflammation: Food was removed after mice were injected with CFA. Paw volume was measured 24 h after the CFA injection. Mice were then given *ad libitum* access to food and paw volume was remeasured after 24 h access to food.

Effect of NSAIDs on CFA-Induced peripheral inflammation: Food was removed after mice were injected with CFA. *Ad libitum* fed mice served as controls. All mice received a subcutaneous injection of 10% ethanol in saline, ketoprofen (30 mg/kg),[64,65] or ketorolac (30 mg/kg)[66,67] 24 h after CFA injection. Doses were picked for their potent analgesic and anti-inflammatory effects. Paw volume was measured 1 h post-i.p. injection.

Effect of chemogenetic AgRP neuron activation on CFA-Induced peripheral inflammation: Mice received an i.p. injection of CNO (1 mg/kg) to activate AgRP neurons 24 h after CFA injection. Paw volume was measured 75 min after CNO administration.

Effect of chemogenetic AgRP neuron inhibition on CFA-Induced peripheral inflammation: Mice were injected with CFA and paw volume was measured 24 h after the injection. Mice were then food deprived overnight for 12 h and paw volume was measured (t = 0). Mice received an i.p. injection of CNO (1 mg/kg) to inhibit AgRP neurons. Paw volume was measured each hour following the i.p. injection. An additional dose of CNO (1 mg/kg) was given 3 h after the initial CNO initial injection.

Effect of optogenetic AgRP neuron stimulation on CFA-Induced peripheral inflammation: Mice received 1 h optogenetic stimulation of AgRP neurons 24 h after CFA injection. Paw volume and temperature were measured immediately after the stimulation. TNFα levels were measured after data collection.

Effect of optogenetic stimulation of AgRP projection subpopulations on CFA-Induced peripheral inflammation: Mice received 1 h optogenetic stimulation of AgRP target subpopulations 24 h after CFA injection. Paw volume and temperature were measured immediately after the stimulation. TNFα levels were measured after data collection.

Effect of vagal signaling on CFA-Induced peripheral inflammation: Sham- and VGX-operated mice were injected with CFA. Paws were measured 24 h post-CFA injection and all mice were subsequently food deprived. Paws were measured again 24 h after food deprivation.

Effect of vagal afferent ablation on CFA-Induced peripheral inflammation: Sham- and capsaicin-treated mice were injected with CFA. Paws were measured 24 h post-CFA injection and all mice were subsequently food deprived. Paws were measured again 24 h after food deprivation.

Effect of vagal efferent antagonism on CFA-Induced peripheral inflammation: Food was removed after mice were injected with CFA. *Ad libitum* fed mice served as controls. Mice received i.p. injections of a mixture of 30 mg/kg antalarmin, 15 μg/kg Astressin 2B, 5 mg/kg mecamylamine, 10 mg/kg propranolol and 5 mg/kg SR59230A or vehicle 24 h post-CFA injection. Paw volume was measured 1 h after administration of adrenergic antagonists.

Inflammatory pain measurements (formalin test)—Mice were placed in a clear enclosure for a 10-min habituation period. Mice were subcutaneously injected in the dorsal hindpaw with 2% formalin (20 μL). Mice were monitored for time spent licking the injected paw, and number of lick bouts, for 1 h post-injection by researchers blinded to experimental condition. All sessions were video-recorded. The time spent paw licking was recorded for 1 h and analyzed during the inflammatory phase (15–45 min).

Effect of AgRP→PBN stimulation on inflammatory pain: Mice received optogenetic stimulation *of* AgRP→PBN neurons beginning 10 min prior to formalin injection and lasting throughout the formalin test. Paw licking was recorded for 1 h post formalin injection. The inflammatory phase of the formalin assay (15–45 min) was analyzed.

Effect of capsaicin-induced vagotomy on inflammatory pain: Sham- and capsaicin-treated mice were injected with formalin in the dorsal hindpaw. Paw licking was recorded for 1 h post formalin injection. The inflammatory phase of the formalin assay (15–45 m) was presented.

Immunohistochemistry and imaging—Mice were transcardially perfused with 0.1 M phosphate buffered saline (PBS) followed by 4% paraformaldehyde (PFA). Brains were removed and post-fixed for 4 h in PFA and then washed overnight in PBS. Coronal brain sections were cut (150 μm sections) on a vibratome or cryostat and stored in PBS. Brain sections were incubated overnight at 4°C with primary antibodies diluted in PBS, 1% BSA and 0.1% Triton X-100. Antibodies used: rabbit anti-cFos (1:5,000, Cell Signaling, 2250), sheep anti-GFP (1:2000, AbD Serotec 4745-1051) goat anti-ChAT (1:2000, Millipore, AB144P). Sections were washed 3 times and incubated with species appropriate and minimally cross-reactive fluorophore-conjugated secondary antibodies (1:500, Jackson ImmunoResearch) for 2 h at room temperature. Sections were washed twice with PBS and mounted and coverslipped with Fluorogel. Epifluorescence images were taken on a Leica stereoscope to verify fiber placements, cannula placements, and to obtain low magnification images. Confocal micrographs were taken on a Leica SPE laser scanning microscope using a 20X, 0.75 NA objective for visualization of Fos immunoreactivity.

QUANTIFICATION AND STATISTICAL ANALYSES

Data were expressed as means ± SEMs in figures and text. Paired or unpaired two-tailed t-tests and Pearson regressions were performed as appropriate. One-way, two-way, and repeated measures ANOVA were used to make comparisons across more than two groups using Prism software. Test, statistics, significance levels, and sample sizes for each experiment are listed in Table S1 ns $p > 0.05$, t-tests and post-hoc comparisons: $^{*}p < 0.05$, $^{**}p < 0.01$, $^{***}p < 0.001$; ANOVA interaction: ∞$p < 0.05$, ∞∞$p < 0.01$, ∞∞∞$p < 0.001$; ANOVA main effect (group, state, or drug): ☼<0.05, ☼☼$p < 0.01$, ☼☼☼$p < 0.001$.

Supplementary Material

Refer to Web version on PubMed Central for supplementary material.

ACKNOWLEDGMENTS

We thank Grant Grothusen for comments on the manuscript. We also thank Jamie Carty, Ella Cho, and Claudia Pichardo for assistance with experiments. We thank Heather Collins, who is supported by P30-DK19525 and S10-OD025098, of the University of Pennsylvania Diabetes Research Center Radioimmunoassay & Biomarkers Core for completion of the radioimmunoassay. K.A.K. is supported by the Center for Undergraduate Research & Fellowships at the University of Pennsylvania. N.G. is supported by the National Science Foundation Graduate Research (DGE-1845298). C.A.A. is supported by the Abramson Cancer Center Support Grant (P30 CA016520) and the instrumentation used by an NIH Shared Instrumentation Grant (S10 OD023465-01A1). A.L.A. is supported by the Monell Chemical Senses Center, NIH (DP2AT011965), the Klingenstein-Simons Foundation Award in Neuroscience, and the American Heart Association (857082) and is a New York Stem Cell Investigator – Robertson Investigator and a Pew Biomedical Scholar. J.N.B. is supported by the University of Pennsylvania School of Arts and Sciences, the American Diabetes Association (118IBS116), the American Heart Association (AHA 17SDG33400158), the Whitehall Foundation, the Klingenstein-Simons Fellowship Award. and the NIH (1R01DK114104 and P01DK088761).

REFERENCES

1. Mattson MP, Longo VD, and Harvie M (2017). Impact of intermittent fasting on health and disease processes. Ageing Res. Rev 39, 46–58. 10.1016/j.arr.2016.10.005. [PubMed: 27810402]
2. Fontana L, Meyer TE, Klein S, and Holloszy JO (2004). Long-term calorie restriction is highly effective in reducing the risk for atherosclerosis in humans. P Natl Acad Sci Usa 101, 6659–6663. 10.1073/pnas.0308291101.
3. Traba J, Kwarteng-Siaw M, Okoli TC, Li J, Huffstutler RD, Bray A, Waclawiw MA, Han K, Pelletier M, Sauve AA, et al. (2015). Fasting and refeeding differentially regulate NLRP3 inflammasome activation in human subjects. J. Clin. Invest 125, 4592–4600. 10.1172/jci83260. [PubMed: 26529255]
4. Traba J, and Sack MN (2017). The role of caloric load and mitochondrial homeostasis in the regulation of the NLRP3 inflammasome. Cell. Mol. Life Sci 74, 1777–1791. 10.1007/s00018-016-2431-7. [PubMed: 27942750]
5. Vandanmagsar B, Youm Y-H, Ravussin A, Galgani JE, Stadler K, Mynatt RL, Ravussin E, Stephens JM, and Dixit VD (2011). The NLRP3 inflammasome instigates obesity-induced inflammation and insulin resistance. Nat. Med 17, 179–188. 10.1038/nm.2279. [PubMed: 21217695]
6. Youm Y-H, Nguyen KY, Grant RW, Goldberg EL, Bodogai M, Kim D, D'Agostino D, Planavsky N, Lupfer C, Kanneganti TD, et al. (2015). The ketone metabolite b-hydroxybutyrate blocks NLRP3 inflammasome–mediated inflammatory disease. Nat. Med 21, 263–269. 10.1038/nm.3804. [PubMed: 25686106]
7. Brandhorst S, Choi IY, Wei M, Cheng CW, Sedrakyan S, Navarrete G, Dubeau L, Yap LP, Park R, Vinciguerra M, et al. (2015). A Periodic Diet that Mimics Fasting Promotes Multi-System Regeneration, Enhanced Cognitive Performance, and Healthspan. Cell Metab 22, 86–99. 10.1016/j.cmet.2015.05.012. [PubMed: 26094889]
8. Meydani SN, Das SK, Pieper CF, Lewis MR, Klein S, Dixit VD, Gupta AK, Villareal DT, Bhapkar M, Huang M, et al. (2016). Long-term moderate calorie restriction inhibits inflammation without impairing cell-mediated immunity: a randomized controlled trial in non-obese humans. Aging Albany Ny 8, 1416–1431. 10.18632/aging.100994. [PubMed: 27410480]
9. Johnson JB, Summer W, Cutler RG, Martin B, Hyun D-H, Dixit VD, Pearson M, Nassar M, Telljohann R, Maudsley S, et al. (2007). Alternate day calorie restriction improves clinical findings and reduces markers of oxidative stress and inflammation in overweight adults with moderate asthma. Free Radic. Biol. Med 42, 665–674. 10.1016/j.freeradbiomed.2006.12.005. [PubMed: 17291990]
10. Wang T, Hung CCY, and Randall DJ (2006). THE COMPARATIVE PHYSIOLOGY OF FOOD DEPRIVATION: From Feast to Famine. Physiology 68, 223–251. 10.1146/annurev.physiol.68.040104.105739.
11. Culbert KM, Racine SE, and Klump KL (2016). Hormonal Factors and Disturbances in Eating Disorders. Curr Psychiat Rep 18, 65. 10.1007/s11920-016-0701-6.
12. Al-Hasani H, and Joost H-G (2005). Nutrition-/diet-induced changes in gene expression in white adipose tissue. Best Pract Res Cl En 19, 589–603. 10.1016/j.beem.2005.07.005.
13. Matarese G, Procaccini C, Menale C, Kim JG, Kim JD, Diano S, Diano N, De Rosa V, Dietrich MO, and Horvath TL (2013). Hunger-promoting hypothalamic neurons modulate effector and regulatory T-cell responses. Proc National Acad Sci 110, 6193–6198. 10.1073/pnas.1210644110.
14. Alhadeff AL, Su Z, Hernandez E, Klima ML, Phillips SZ, Holland RA, Guo C, Hantman AW, De Jonghe BC, and Betley JN (2018). A Neural Circuit for the Suppression of Pain by a Competing Need State. Cell 173, 140–152.e15. 10.1016/j.cell.2018.02.057. [PubMed: 29570993]
15. Kovats S, Carreras E, and Agrawal H (2009). Sex Hormones and Immunity to Infection, pp. 53–91. 10.1007/978-3-642-02155-8_3.
16. Klein SL, and Flanagan KL (2016). Sex differences in immune responses. Nat. Rev. Immunol 16, 626–638. 10.1038/nri.2016.90. [PubMed: 27546235]
17. Doyle HH, and Murphy AZ (2017). Sex differences in innate immunity and its impact on opioid pharmacology. J. Neurosci. Res 95, 487–499. 10.1002/jnr.23852. [PubMed: 27870418]

18. Cook CD, and Nickerson MD (2005). Nociceptive Sensitivity and Opioid Antinociception and Antihyperalgesia in Freund's Adjuvant-Induced Arthritic Male and Female Rats. J. Pharmacol. Exp. Ther 313, 449–459. 10.1124/jpet.104.077792. [PubMed: 15608071]
19. Shaw AC, Goldstein DR, and Montgomery RR (2013). Age-dependent dysregulation of innate immunity. Nat. Rev. Immunol 13, 875–887. 10.1038/nri3547. [PubMed: 24157572]
20. Taniguchi K, and Karin M (2018). NF-kB, inflammation, immunity and cancer: coming of age. Nat. Rev. Immunol 18, 309–324. 10.1038/nri.2017.142. [PubMed: 29379212]
21. Wellen KE, and Hotamisligil GS (2005). Inflammation, stress, and diabetes. J. Clin. Invest 115, 1111–1119. 10.1172/jci25102. [PubMed: 15864338]
22. Nathan C (2002). Points of control in inflammation. Nature 420, 846–852. 10.1038/nature01320. [PubMed: 12490957]
23. Medzhitov R (2008). Origin and physiological roles of inflammation. Nature 454, 428–435. 10.1038/nature07201. [PubMed: 18650913]
24. Oliveira PG, Brenol CV, Edelweiss MI, Meurer L, Brenol JCT, and Xavier RM (2007). Subcutaneous inflammation (panniculitis) in tibiotarsal joint of rats inoculated with complete Freund's adjuvant. Clin. Exp. Med 7, 184–187. 10.1007/s10238-007-0148-6. [PubMed: 18188533]
25. Berthoud H-R, and Neuhuber WL (2000). Functional and chemical anatomy of the afferent vagal system. Auton. Neurosci 85, 1–17. 10.1016/s1566-0702(00)00215-0. [PubMed: 11189015]
26. Yuan H, and Silberstein SD (2016). Vagus Nerve and Vagus Nerve Stimulation, a Comprehensive Review: Part I. Headache J. Head Face Pain 56, 71–78. 10.1111/head.12647.
27. Goehler LE, Gaykema RP, Hansen MK, Anderson K, Maier SF, and Watkins LR (2000). Vagal immune-to-brain communication: a visceral chemosensory pathway. Auton. Neurosci 85, 49–59. 10.1016/s1566-0702(00)00219-8. [PubMed: 11189026]
28. Craig AD, and Bud. (2003). Interoception: the sense of the physiological condition of the body. Curr. Opin. Neurobiol 13, 500–505. 10.1016/s0959-4388(03)00090-4. [PubMed: 12965300]
29. Bonaz B, Sinniger V, and Pellissier S (2017). The Vagus Nerve in the Neuro-Immune Axis: Implications in the Pathology of the Gastrointestinal Tract. Front. Immunol 8, 1452. 10.3389/fimmu.2017.01452. [PubMed: 29163522]
30. Berthoud H-R, Patterson LM, Neumann F, and Neuhuber WL (1997). Distribution and structure of vagal afferent intraganglionic laminar endings (IGLEs) in the rat gastrointestinal tract. Anat. Embryol 195, 183–191. 10.1007/s004290050037.
31. Holzer P (1991). Capsaicin: cellular targets, mechanisms of action, and selectivity for thin sensory neurons. Pharmacol. Rev 43, 143–201. [PubMed: 1852779]
32. Cowley MA, Smith RG, Diano S, Tschöp M, Pronchuk N, Grove KL, Strasburger CJ, Bidlingmaier M, Esterman M, Heiman ML, et al. (2003). The Distribution and Mechanism of Action of Ghrelin in the CNS Demonstrates a Novel Hypothalamic Circuit Regulating Energy Homeostasis. Neuron 37, 649–661. 10.1016/s0896-6273(03)00063-1. [PubMed: 12597862]
33. Takahashi KA, and Cone RD (2005). Fasting Induces a Large, Leptin-Dependent Increase in the Intrinsic Action Potential Frequency of Orexigenic Arcuate Nucleus Neuropeptide Y/Agouti-Related Protein Neurons. Endocrinology 146, 1043–1047. 10.1210/en.2004-1397. [PubMed: 15591135]
34. Yang Y, Atasoy D, Su HH, and Sternson SM (2011). Hunger States Switch a Flip-Flop Memory Circuit via a Synaptic AMPK-Dependent Positive Feedback Loop. Cell 146, 992–1003. 10.1016/j.cell.2011.07.039. [PubMed: 21925320]
35. Liu T, Kong D, Shah BP, Ye C, Koda S, Saunders A, Ding JB, Yang Z, Sabatini BL, and Lowell BB (2012). Fasting activation of AgRP neurons requires NMDA receptors and involves spinogenesis and increased excitatory tone. Neuron 73, 511–522. 10.1016/j.neuron.2011.11.027. [PubMed: 22325203]
36. Krashes MJ, Koda S, Ye C, Rogan SC, Adams AC, Cusher DS, Maratos-Flier E, Roth BL, and Lowell BB (2011). Rapid, reversible activation of AgRP neurons drives feeding behavior in mice. J. Clin. Invest 121, 1424–1428. 10.1172/jci46229. [PubMed: 21364278]
37. Betley JN, Cao ZFH, Ritola KD, and Sternson SM (2013). Parallel, redundant circuit organization for homeostatic control of feeding behavior. Cell 155, 1337–1350. 10.1016/j.cell.2013.11.002. [PubMed: 24315102]

38. Broberger C, Johansen J, Johansson C, Schalling M, and Hökfelt T (1998). The neuropeptide Y/agouti gene-related protein (AGRP) brain circuitry in normal, anorectic, and monosodium glutamate-treated mice. Proc National Acad Sci 95, 15043–15048. 10.1073/pnas.95.25.15043.
39. Alhadeff AL, Park O, Hernandez E, and Betley JN (2020). Inhibition of Itch by Hunger and AgRP Neuron Activity. Neuroscience 450, 126–134. 10.1016/j.neuroscience.2020.06.005. [PubMed: 32540365]
40. Aponte Y, Atasoy D, and Sternson SM (2011). AGRP neurons are sufficient to orchestrate feeding behavior rapidly and without training. Nat. Neurosci 14, 351–355. 10.1038/nn.2739. [PubMed: 21209617]
41. Betley JN, Xu S, Cao ZFH, Gong R, Magnus CJ, Yu Y, and Sternson SM (2015). Neurons for hunger and thirst transmit a negative-valence teaching signal. Nature 521, 180–185. 10.1038/nature14416. [PubMed: 25915020]
42. Burnett CJ, Li C, Webber E, Tsaousidou E, Xue SY, Brüning JC, and Krashes MJ (2016). Hunger-Driven Motivational State Competition. Neuron 92, 187–201. 10.1016/j.neuron.2016.08.032. [PubMed: 27693254]
43. Dietrich M, Zimmer M, Bober J, and Horvath T (2015). Hypothalamic Agrp Neurons Drive Stereotypic Behaviors beyond Feeding
44. Goldstein N, Levine BJ, Loy KA, Duke WL, Meyerson OS, Jamnik AA, and Carter ME (2018). Hypothalamic Neurons that Regulate Feeding Can Influence Sleep/Wake States Based on Homeostatic Need. Curr. Biol 28, 3736–3747.e3. 10.1016/j.cub.2018.09.055. [PubMed: 30471995]
45. Jikomes N, Ramesh RN, Mandelblat-Cerf Y, and Andermann ML (2016). Preemptive Stimulation of AgRP Neurons in Fed Mice Enables Conditioned Food Seeking under Threat. Curr. Biol 26, 2500–2507. 10.1016/j.cub.2016.07.019. [PubMed: 27568593]
46. Padilla SL, Qiu J, Soden ME, Sanz E, Nestor CC, Barker FD, Quintana A, Zweifel LS, Rønnekleiv OK, Kelly MJ, and Palmiter RD (2016). Agouti-related peptide neural circuits mediate adaptive behaviors in the starved state. Nat. Neurosci 19, 734–741. 10.1038/nn.4274. [PubMed: 27019015]
47. de Araujo Salgado I, Li C, Burnett CJ, Rodriguez Gonzalez S, Becker JJ, Horvath A, Earnest T, Kravitz AV, and Krashes MJ (2023). Toggling between food-seeking and self-preservation behaviors via hypothalamic response networks. Neuron 111, 2899–2917.e6. 10.1016/j.neuron.2023.06.006. [PubMed: 37442130]
48. Könner AC, Janoschek R, Plum L, Jordan SD, Rother E, Ma X, Xu C, Enriori P, Hampel B, Barsh GS, et al. (2007). Insulin Action in AgRP-Expressing Neurons Is Required for Suppression of Hepatic Glucose Production. Cell Metab 5, 438–449. 10.1016/j.cmet.2007.05.004. [PubMed: 17550779]
49. Steculorum SM, Ruud J, Karakasilioti I, Backes H, Engström Ruud L, Timper K, Hess ME, Tsaousidou E, Mauer J, Vogt MC, et al. (2016). AgRP Neurons Control Systemic Insulin Sensitivity via Myostatin Expression in Brown Adipose Tissue. Cell 165, 125–138. 10.1016/j.cell.2016.02.044. [PubMed: 27015310]
50. Douglass AM, Resch JM, Madara JC, Kucukdereli H, Yizhar O, Grama A, Yamagata M, Yang Z, and Lowell BB (2023). Neural basis for fasting activation of the hypothalamic–pituitary–adrenal axis. Nature 620, 154–162. 10.1038/s41586-023-06358-0. [PubMed: 37495689]
51. Fernandes ACA, de Oliveira FP, Antunes-Rodrigues J, Fernandez G, da Guia Vieira L, Rosa CG, do Nascimento T, de Castro França S, Donato J, et al. (2022). Arcuate AgRP, but not POMC neurons, modulate paraventricular CRF synthesis and release in response to fasting. Cell Biosci 12, 118. 10.1186/s13578-022-00853-z. [PubMed: 35902915]
52. Bell BB, Harlan SM, Morgan DA, Guo D-F, Cui H, and Rahmouni K (2018). Differential contribution of POMC and AgRP neurons to the regulation of regional autonomic nerve activity by leptin. Mol. Metab 8, 1–12. 10.1016/j.molmet.2017.12.006. [PubMed: 29289646]
53. Essner RA, Smith AG, Jamnik AA, Ryba AR, Trutner ZD, and Carter ME (2017). AgRP Neurons Can Increase Food Intake during Conditions of Appetite Suppression and Inhibit Anorexigenic Parabrachial Neurons. J. Neurosci 37, 8678–8687. 10.1523/jneurosci.0798-17.2017. [PubMed: 28821663]
54. Wu Q, Clark MS, and Palmiter RD (2012). Deciphering a neuronal circuit that mediates appetite. Nature 483, 594–597. 10.1038/nature10899. [PubMed: 22419158]

55. Waldburger J-M, and Firestein GS (2010). Regulation of Peripheral Inflammation by the Central Nervous System. Curr. Rheumatol. Rep 12, 370–378. 10.1007/s11926-010-0124-z. [PubMed: 20676807]
56. Tong Q, Ye C-P, Jones JE, Elmquist JK, and Lowell BB (2008). Synaptic release of GABA by AgRP neurons is required for normal regulation of energy balance. Nat. Neurosci 11, 998–1000. 10.1038/nn.2167. [PubMed: 19160495]
57. Madisen L, Mao T, Koch H, Zhuo J.m., Berenyi A, Fujisawa S, Hsu Y-WA, Garcia AJ, Gu X, Zanella S, et al. (2012). A toolbox of Cre-dependent optogenetic transgenic mice for light-induced activation and silencing. Nat. Neurosci 15, 793–802. 10.1038/nn.3078. [PubMed: 22446880]
58. Zhu H, Aryal DK, Olsen RHJ, Urban DJ, Swearingen A, Forbes S, Roth BL, and Hochgeschwender U (2016). Cre-dependent DREADD (Designer Receptors Exclusively Activated by Designer Drugs) mice. genesis 54, 439–446. 10.1002/dvg.22949. [PubMed: 27194399]
59. Alhadeff AL, Goldstein N, Park O, Klima ML, Vargas A, and Betley JN (2019). Natural and Drug Rewards Engage Distinct Pathways that Converge on Coordinated Hypothalamic and Reward Circuits. Neuron 103, 891–908.e6. 10.1016/j.neuron.2019.05.050. [PubMed: 31277924]
60. Carey LM, Gutierrez T, Deng L, Lee W-H, Mackie K, and Hohmann AG (2017). Inflammatory and Neuropathic Nociception is Preserved in GPR55 Knockout Mice. Sci. Rep 7, 944. 10.1038/s41598-017-01062-2. [PubMed: 28428628]
61. Hamm RJ, and Lyeth BG (1984). Nociceptive thresholds following food restriction and return to free-feeding. Physiol. Behav 33, 499–501. 10.1016/0031-9384(84)90176-8. [PubMed: 6514838]
62. Hunskaar S, and Hole K (1987). The formalin test in mice: dissociation between inflammatory and non-inflammatory pain. Pain 30, 103–114. 10.1016/0304-3959(87)90088-1. [PubMed: 3614974]
63. Marchand F, Perretti M, and McMahon SB (2005). Role of the Immune system in chronic pain. Nat. Rev. Neurosci 6, 521–532. 10.1038/nrn1700. [PubMed: 15995723]
64. Girard P, Verniers D, Coppé MC, Pansart Y, and Gillardin J-M (2008). Nefopam and ketoprofen synergy in rodent models of antinociception. Eur. J. Pharmacol 584, 263–271. 10.1016/j.ejphar.2008.02.012. [PubMed: 18316069]
65. Costa SKPF, Muscara MN, Allain T, Dallazen J, Gonzaga L, Buret AG, Vaughan DJ, Fowler CJ, de Nucci G, and Wallace JL (2020). Enhanced Analgesic Effects and Gastrointestinal Safety of a Novel, Hydrogen Sulfide-Releasing Anti-Inflammatory Drug (ATB-352): A Role for Endogenous Cannabinoids. Antioxid Redox Sign 33, 1003–1009. 10.1089/ars.2019.7884.
66. Shin J-W, Hwang K-S, Kim Y-K, Leem J-G, and Lee C (2006). Nonsteroidal Antiinflammatory Drugs Suppress Pain-Related Behaviors, but Not Referred Hyperalgesia of Visceral Pain in Mice. Anesth. Analg 102, 195–200. 10.1213/01.ane.0000184828.39754.a3. [PubMed: 16368829]
67. Russo R, De Caro C, Avallone B, Magliocca S, Nieddu M, Boatto G, Troiano R, Cuomo R, Cirillo C, Avagliano C, et al. (2017). Ketogal: A Derivative Ketorolac Molecule with Minor Ulcerogenic and Renal Toxicity. Front. Pharmacol 8, 757. 10.3389/fphar.2017.00757. [PubMed: 29163153]

Highlights

- Hunger induces an anti-inflammatory effect more potent than NSAIDs
- Anti-inflammatory effects of hunger require descending vagal signaling
- Activity in hunger-activated AgRP→PVH neurons reduces inflammation

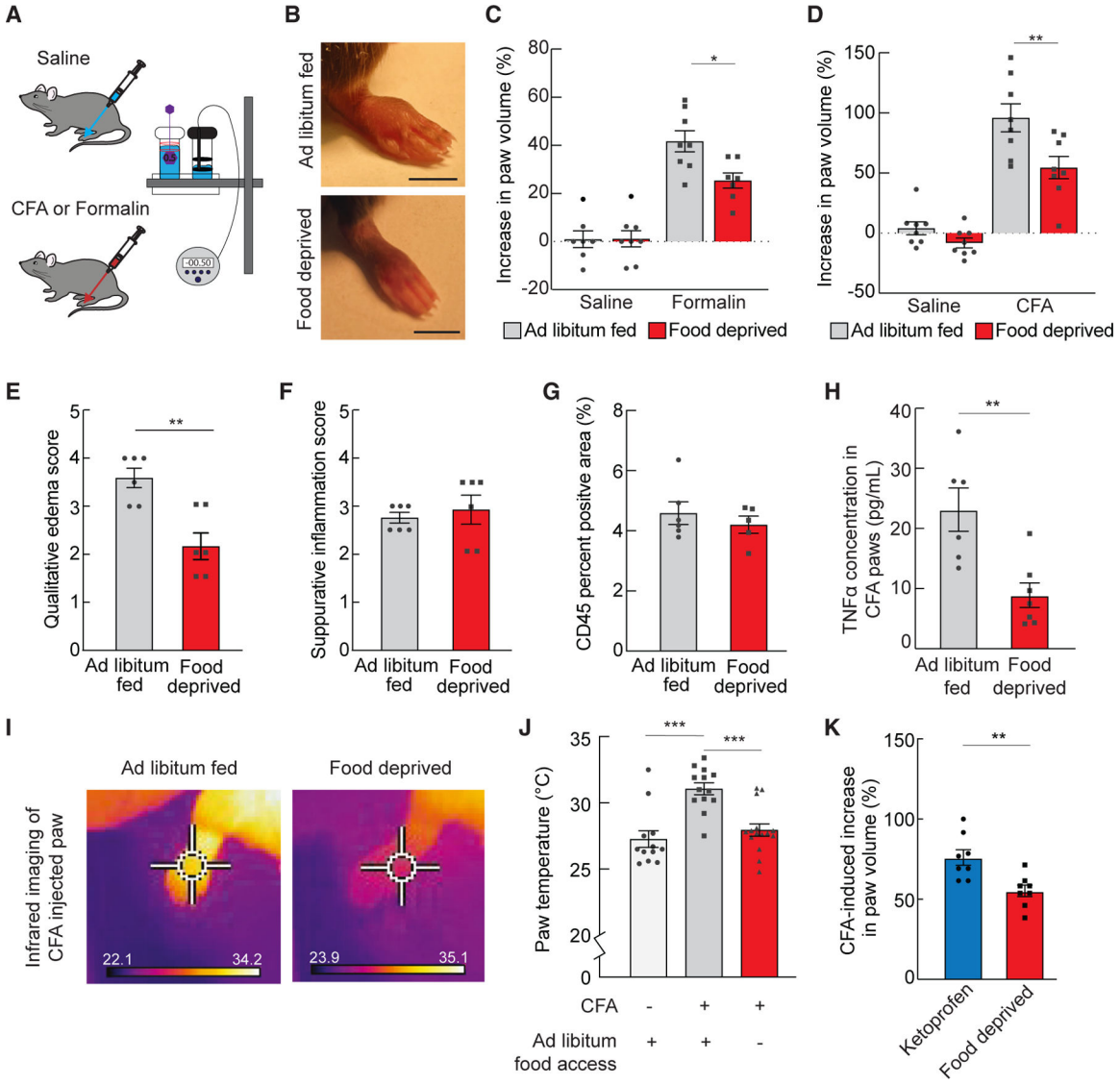

Figure 1. Hunger reduces paw inflammation induced by CFA or formalin

(A) Experimental design: mice were injected with saline, CFA, or formalin, and paw volume was measured using a plethysmometer at various time points post-injection.

(B) Images of paws 24 h after CFA injection followed by *ad libitum* access or 24 h food deprivation. Scale bar, 5 mm.

(C) Increase in paw volume of *ad libitum*-fed (n = 8) and 24-h-food-deprived (n = 8) mice 1 h after a saline or formalin injection (two-way ANOVA, main effect of *ad libitum* fed vs. food deprived p = 0.027).

(D) Increase in paw volume of *ad libitum*-fed (n = 8) and 24-h-food-deprived (n = 8) mice 24 h after a saline or CFA injection (two-way ANOVA, main effect of *ad libitum* fed vs. food deprived p = 0.008).

(E) Qualitative edema score from paw histology analysis of *ad libitum*-fed (n = 6) and 24-h-food-deprived (n = 6) mice 24 h after a CFA injection (unpaired t test, p = 0.002).

(F) Qualitative suppurative inflammation score from paw histology analysis of *ad libitum*-fed (n = 6) and 24-h-food-deprived (n = 6) mice 24 h after a CFA injection (unpaired t test, p = 0.614).
(G) $CD45^+$ area in *ad libitum*-fed (n = 6) and 24-h-food-deprived (n = 5) mice 24 h after a CFA injection (unpaired t test, p = 0.430).
(H) Concentration of TNF-α detected in paws 24 h after CFA injection in *ad libitum*-fed (n = 6) or 24-h-food-deprived (n = 7) mice (unpaired t test, p = 0.004).
(I) Infrared images of paws 24 h after injection with CFA in *ad libitum*-fed and 24-h-food-deprived conditions.
(J) Paw temperature of mice without a CFA injection (n = 13) and 24 h after a CFA injection in *ad libitum*-fed (n = 12) and 24-h-food-deprived states (n = 15) (one-way ANOVA, p < 0.001).
(K) Increase in paw volume of mice (n = 8) 24 h after a CFA injection in *ad libitum*-fed mice treated with 30 mg/kg ketoprofen or 24-h-food-deprived mice treated with vehicle (paired t test, p = 0.003).
Data are expressed as mean ± SEM; t test and post hoc comparisons: $^*p < 0.05$, $^{**}p < 0.01$, $^{***}p < 0.001$.

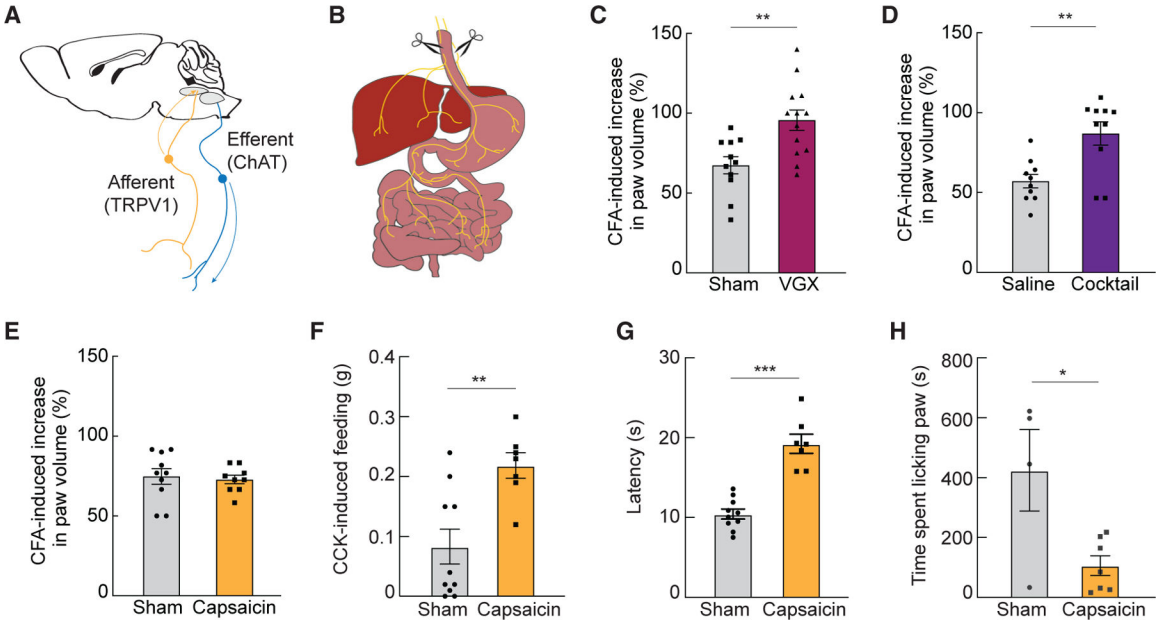

Figure 2. Vagal efferent signaling mediates the effect of hunger on peripheral inflammation

(A) Diagram of ChAT-expressing vagal efferents and capsaicin-sensitive TRPV1-expressing vagal afferents.

(B) Diagram of subdiaphragmatic vagotomy (VGX) surgical procedure.

(C) Increase in paw volume of sham (n = 11) and VGX (n = 13) mice during food deprivation (unpaired t test, p = 0.033).

(D) Increase in paw volume of food-deprived mice systemically treated with saline (n = 10) or a cocktail of CRF, adrenergic, and cholinergic antagonists (n = 10) to block efferent vagal signaling (unpaired t test, p = 0.002).

(E) Increase in paw volume of food-deprived mice systemically treated with vehicle (sham, n = 10) or capsaicin (n = 9) (unpaired t test, p = 0.736).

(F) CCK-induced feeding in sham- (n = 10) or capsaicin-treated mice (n = 8) after 24 h food deprivation (unpaired t test, p = 0.004).

(G) Latency to paw withdraw of sham- (n = 10) or capsaicin-treated mice (n = 8) on 52°C hot plate (unpaired t test, $p < 0.001$).

(H) Time spent licking paw during the inflammatory phase (15–45 min post-injection) of the formalin pain assay in sham- (n = 4) and capsaicin-treated mice (n = 7) (unpaired t test, p = 0.040).

Data are expressed as mean ± SEM; t test: $^{*}p < 0.05$, $^{**}p < 0.01$, $^{***}p < 0.001$.

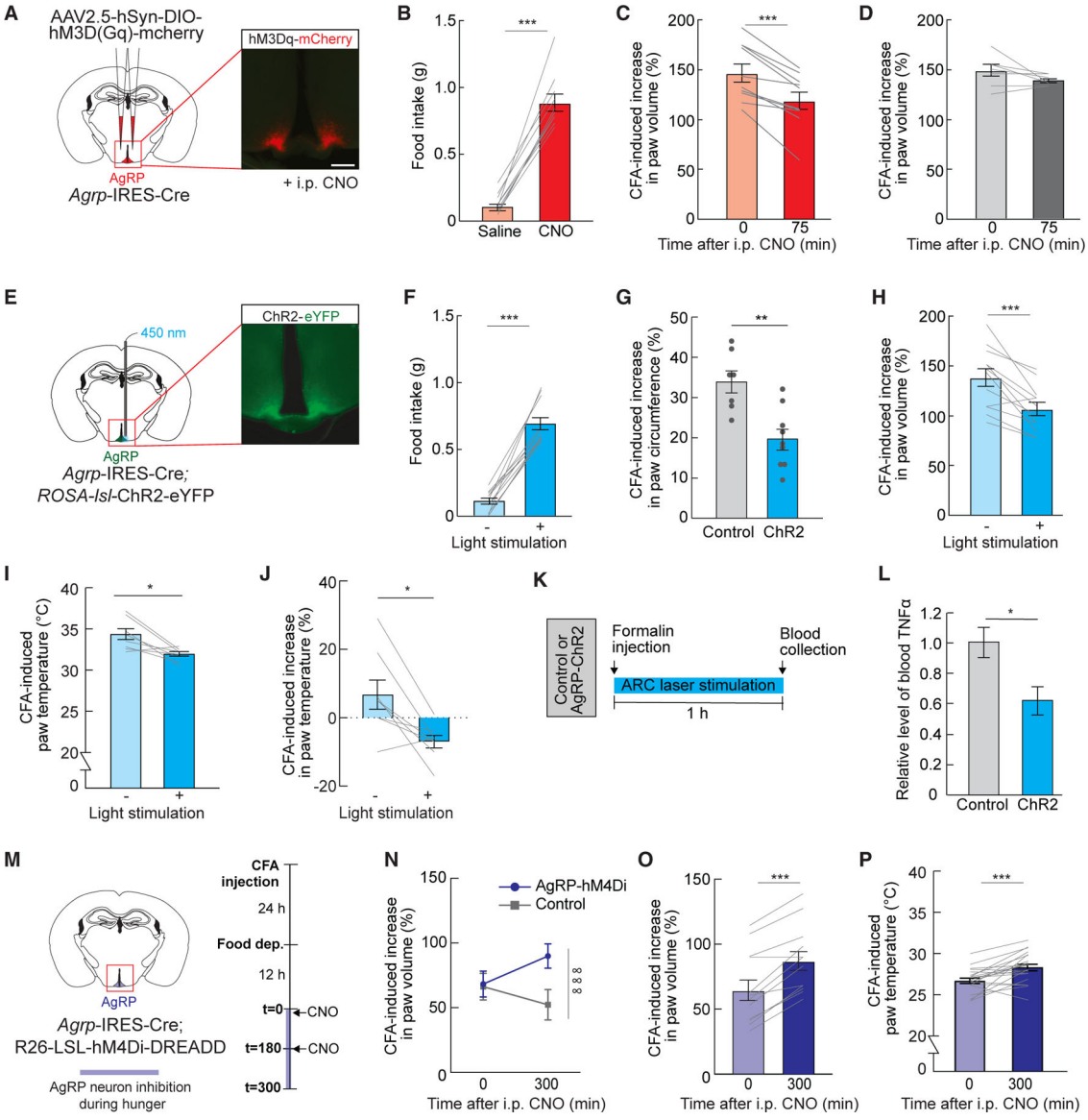

Figure 3. AgRP neuron activity reduces peripheral paw inflammation

(A) Schematic and representative image of Cre-dependent hM3Dq-mCherry expression in AgRP-IRES-cre mice. Scale bar, 200 μm.

(B) 60 min food intake measurement following intraperitoneal (i.p.) saline or 1 mg/kg clozapine-N-oxize (CNO) administration in *ad libitum*-fed AgRP hM3Dq-expressing (n = 10) mice (paired t test, $p < 0.001$).

(C) Increase in paw volume 24 h after CFA injection in *ad libitum*-fed AgRP hM3Dq-expressing (n = 10) mice before and 75 min after 1 mg/kg CNO administration (paired t test, $p < 0.001$).

(D) Increase in paw volume 24 h after CFA injection in *ad libitum*-fed control AgRP mCherry-expressing (n = 7) mice before and 75 min after 1 mg/kg CNO administration (paired t test, $p = 0.153$).

(E) Schematic and representative image of Cre-dependent ChR2-EYFP expression in Ai32 x AgRP-IRES-Cre mice with an optical fiber over the arcuate hypothalamic nucleus (ARC) to selectively activate AgRP neurons. Scale bar, 200 μm.
(F) 60 min food intake measurements without (−) and with (+) optogenetic stimulation in *ad libitum*-fed AgRP ChR2-expressing (n = 12) mice (paired t test, $p < 0.001$).
(G) Increase in paw circumference 24 h after CFA injection in *ad libitum*-fed control (n = 7) and AgRP ChR2-expressing (n = 9) mice (unpaired t test, $p < 0.01$).
(H) Increase in paw volume 24 h after CFA injection in *ad libitum*-fed AgRP ChR2-expressing (n = 12) mice before (−) and after (+) 60 min optogenetic stimulation (paired t test, $p < 0.001$).
(I) Paw temperature 24 h after CFA injection of *ad libitum*-fed AgRP ChR2-expressing mice (n = 8) before (−) and after (+) 1 h optogenetic stimulation (paired t test, $p = 0.010$).
(J) Percentage of change in paw temperature before (−) and after (+) 1 h optogenetic stimulation (paired t test, $p = 0.010$).
(K) Experimental timeline: control or AgRP ChR2-expressing mice were injected with formalin and given laser stimulation for 1 h before blood collection.
(L) Relative levels of blood TNF-α following 1 h laser stimulation to control (n = 6) or AgRP ChR2-expressing (n = 6) mice (unpaired t tests, $p < 0.05$).
(M) Schematic and experimental timeline of AgRP neuron inhibition during hunger.
(N) Increase in CFA-induced paw volume in AgRP-hM4Di mice (n = 13) and wild-type controls (n = 8) following 12 h food deprivation (0 min) and 5 h after 1 mg/kg CNO administration (300 min) (two-way ANOVA, $p < 0.001$).
(O) Increase in paw volume in AgRP-hM4Di mice (n = 13) before and 300 min after initial CNO administration (paired t test, $p < 0.001$).
(P) Paw temperature in AgRP-hM4Di mice (n = 13) before and 300 min after initial CNO administration (paired t test, $p < 0.001$).
Data are expressed as mean ± SEM; t tests: $^{*}p < 0.05$, $^{**}p < 0.01$, $^{***}p < 0.001$; two-way ANOVA interaction: $^{\infty\infty\infty\infty}p < 0.001$.

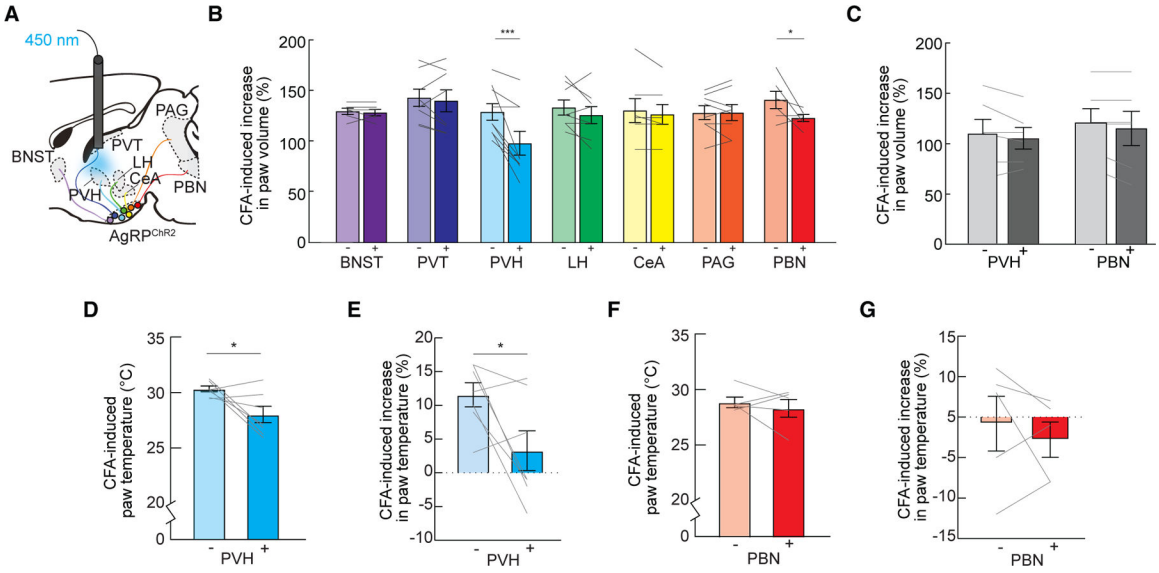

Figure 4. AgRP→PVH and AgRP→PBN neuron activity suppresses CFA-induced paw inflammation

(A) Diagram of the major AgRP projection subpopulations analyzed. Delivery of light to individual axon target fields of ChR2-expressing AgRP neurons (PVH shown here) allows for selective activation of discrete AgRP neuron projection subpopulations.

(B) Increase in paw volume 24 h after a CFA injection in mice before (−) and after (+) 1 h optogenetic stimulation of AgRP neuron projection subpopulations (n = 6–9/group, two-way mixed-effects ANOVA, Holm-Sidak post hoc, PVH $p < 0.001$, PBN $p = 0.045$, all other structures p = ns).

(C) Increase in paw volume 24 h after a CFA injection of mice before (−) or after (+) 1 h light exposure to AgRP neuron projection subpopulations with control expression of tdTomato (n = 6/group, two-way mixed-effects ANOVA, $p = 0.863$).

(D) Paw temperature 24 h after CFA injection in mice (n = 6) before (−) and after (+) 1 h optogenetic stimulation of AgRP neuron projections in the PVH (paired t test, $p = 0.044$).

(E) Percentage of change in paw temperature before (−) and after (+) 1 h optogenetic stimulation of AgRP neuron projections in the PVH (n = 7) (paired t test, $p = 0.049$).

(F) Paw temperature 24 h after CFA injection in mice (n = 5) before (−) and after (+) 1 h optogenetic stimulation of AgRP neuron projections in the PBN (paired t test, $p = 0.563$).

(G) Percent change in paw temperature before (−) and after (+) 1 h optogenetic stimulation of AgRP neuron projections in the PBN (n = 5) (paired t test, $p = 0.521$).

Data are expressed as mean ± SEM; t test and post-hoc comparisons: $^{*}p < 0.05$, $^{***}p < 0.001$.

KEY RESOURCES TABLE

REAGENT or RESOURCE	SOURCE	IDENTIFIER
Antibodies		
Rabbit anti-cFos	Cell Signaling	2250; RRID:AB_2247211
Goat anti-ChAT	Millipore	AB144P; RRID:AB_2079751
Rat anti CD45-LCA	BD Biosciences	553076; RRID:AB_394606
Fluorescein (FITC) AffiniPure Donkey Anti-Rabbit IgG (H + L)	Jackson ImmunoResearch	711-095-152; RRID:AB_2315776
Cy3 AffiniPure Donkey Anti-Rabbit IgG (H + L)	Jackson ImmunoResearch	711-165-152; RRID:AB_2307443
Cy3 AffiniPure Donkey Anti-Goat IgG (H + L)	Jackson ImmunoResearch	705-175-147; RRID:AB_2340415
ImmPRESS HRP Goat Anti-Rat IgG	Vector Laboratories	MP-7444; RRID:AB_2336530
Bacterial and Virus Strains		
AAV1.CAGGS.flex.ChR2-tdTomato.WPRE.SV40	University of Pennsylvania Vector Core	AV-1-18917P
AAV5.hSyn-DIO-mCherry	Addgene	50459-AAV5
AAV2.5.hSyn-DIO-hM3D(Gq)-mCherry	Addgene	44361-AAV5
Chemicals, peptides, and recombinant proteins		
Dulbecco’s phosphate-buffered saline	HyClone	SH30013.04
Bovine Serum Albumin	Sigma-Aldrich	A9418
Triton X-100	Sigma-Aldrich	93443
Paraformaldehyde	MP Biomedicals	150146
Isoflurane	Clipper	10250
Meloxicam	Norbrook Laboratories	55529-040-11
Bupivicaine	Moore Medical	52683
Hydrogen peroxide	Ricca Chemical Company	R3821310-1BV
Clozapine-N-Oxide	Tocris	4936
Sterile saline	Pfizer	00409-4888-12
Formalin	Sigma-Aldrich	HT50-1-2
Freund’s Adjuvant, Complete	Sigma-Aldrich	F5881
Ketoprofen	Santa Cruz Animal Health	sc-363115Rx
Keterolac	Fisher Scientific	K00531G
Capsaicin	Tocris	462
Antalarmin hydrochloride	Sigma-Aldrich	A8727
Astressin 2B	Tocris	2391
SR 59230A	Sigma-Aldrich	S8688
(+)-Propranolol hydrochloride	Sigma-Aldrich	P0884
Mecamylamine hydrochloride	Tocris	2843
PMSF Protease Inhibitor	ThermoFisher Scientific	36978
Tissue Extraction Reagent I	ThermoFisher Scientific	FNN0071
Fluoro-Gold	Fluorochrome	

REAGENT or RESOURCE	SOURCE	IDENTIFIER
BOND Epitope Retrieval Solution 2	Leica Biosystems	AR9640
PowerVision IHC/ISH Super Blocking solution	Leica Biosystems	PV6122
Diaminobenzidine	N/A	N/A
Hematoxylin	N/A	N/A
Xylene	N/A	N/A
Formic Acid	N/A	N/A
Experimental models: Organisms/strains		
Mouse: Agrp-Ires-cre, Agrp$^{tm1(cre)Lowl}$/J	The Jackson Laboratory	12899
Mouse: Ai32, B6; 129S-*Gt(ROSA)26Sor*$^{tm32(CAG-COP4*H134R/EYFP)Hze}$/J	The Jackson Laboratory	12569
Mouse: C57BL/6J	The Jackson Laboratory	664
Mouse: AgRP-hM4Di, B6N.129-Gt(ROSA) 26Sor$^{tm1(CAG-CHRM4*-mCitrine)/Ute}$/J	The Jackson Laboratory	26219
Mouse: CD1	Charles River	022
Software and algorithms		
Aperio ImageScope	Leica Biosystems	https://www.leicabiosystems.com/us/digital-pathology/manage/aperio-imagescope/
Other		
Microliter syringe pump, PHD Ultra	Harvard Apparatus	703007
Optogenetic fiber	ThorLabs	FT200UMT
1.25 mm zirconia ferrules	Kientech	FZI-LC-230
Metabond	Parkell	S380
Ortho-jet BCA Liquid	Lang Dental Manufacturing	B1306
Jet Tooth Shade Powder	Lang Dental Manufacturing	143069
Guide cannulae	Plastics One	8IC315GS5SPC
Internal cannulae	Plastics One	8IC315IS5SPC
Dummy cannulae	Plastics One	8IC315DCSXXC
Plethysmometer	Ugo Basile	37140
BeadBug microtube homogenizer	Sigma-Aldrich	Z763713
Prefilled 2.0mL tubes, Zirconium Beads	Thomas Scientific	1211U68
Mouse TNF-alpha Quantikine ELISA Kit	R&D Systems	MTA00B
Bond Polymer Refine Detection kit	Leica	DS9800
Epredia ClearVue coverslipper	Fisher Scientific	A79200001
Thermal imaging camera	Teledyne FLIR	T450sc
Aperio AT2	Leica Biosystems	N/A